Dysregulation of ubiquitin homeostasis and β-catenin signaling promote spinal muscular atrophy

Thomas M. Wishart,[1,2] Chantal A. Mutsaers,[1,3] Markus Riessland,[4] Michell M. Reimer,[1,5]
Gillian Hunter,[1,3] Marie L. Hannam,[6] Samantha L. Eaton,[2] Heidi R. Fuller,[7] Sarah L. Roche,[1,3]
Eilidh Somers,[1,3] Robert Morse,[8] Philip J. Young,[8] Douglas J. Lamont,[9] Matthias Hammerschmidt,[10]
Anagha Joshi,[11] Peter Hohenstein,[11] Glenn E. Morris,[7] Simon H. Parson,[1,12] Paul A. Skehel,[1,3]
Thomas Becker,[1,5] Iain M. Robinson,[6] Catherina G. Becker,[1,5]
Brunhilde Wirth,[4] and Thomas H. Gillingwater[1,3]

[1]Euan MacDonald Centre for Motor Neurone Disease Research, University of Edinburgh, Edinburgh, United Kingdom.
[2]Division of Neurobiology, The Roslin Institute and Royal (Dick) School of Veterinary Studies, University of Edinburgh, Edinburgh, United Kingdom.
[3]Centre for Integrative Physiology, University of Edinburgh, Edinburgh, United Kingdom. [4]Institute of Human Genetics,
Institute for Genetics and Center for Molecular Medicine Cologne, University of Cologne, Cologne, Germany. [5]Centre for Neuroregeneration,
University of Edinburgh, Edinburgh, United Kingdom. [6]Peninsula College of Medicine and Dentistry (Universities of Exeter and Plymouth),
John Bull Building, Research Way, Tamar Science Park, Plymouth, United Kingdom. [7]Wolfson Centre for Inherited Neuromuscular Disease,
RJAH Orthopaedic Hospital, Oswestry, United Kingdom, and Institute for Science and Technology in Medicine, Keele University, Keele, United Kingdom.
[8]Peninsula College of Medicine and Dentistry, University of Exeter, Exeter, United Kingdom. [9]Fingerprints Proteomics Facility, Dundee University,
Dundee, United Kingdom. [10]Institute of Developmental Biology, University of Cologne, Cologne, Germany. [11]Division of Developmental Biology,
The Roslin Institute and Royal (Dick) School of Veterinary Studies, University of Edinburgh, Edinburgh, United Kingdom.
[12]Institute of Medical Sciences, School of Medicine and Dentistry, University of Aberdeen, Aberdeen, United Kingdom.

The autosomal recessive neurodegenerative disease spinal muscular atrophy (SMA) results from low levels of survival motor neuron (SMN) protein; however, it is unclear how reduced SMN promotes SMA development. Here, we determined that ubiquitin-dependent pathways regulate neuromuscular pathology in SMA. Using mouse models of SMA, we observed widespread perturbations in ubiquitin homeostasis, including reduced levels of ubiquitin-like modifier activating enzyme 1 (UBA1). SMN physically interacted with UBA1 in neurons, and disruption of *Uba1* mRNA splicing was observed in the spinal cords of SMA mice exhibiting disease symptoms. Pharmacological or genetic suppression of UBA1 was sufficient to recapitulate an SMA-like neuromuscular pathology in zebrafish, suggesting that UBA1 directly contributes to disease pathogenesis. Dysregulation of UBA1 and subsequent ubiquitination pathways led to β-catenin accumulation, and pharmacological inhibition of β-catenin robustly ameliorated neuromuscular pathology in zebrafish, *Drosophila*, and mouse models of SMA. UBA1-associated disruption of β-catenin was restricted to the neuromuscular system in SMA mice; therefore, pharmacological inhibition of β-catenin in these animals failed to prevent systemic pathology in peripheral tissues and organs, indicating fundamental molecular differences between neuromuscular and systemic SMA pathology. Our data indicate that SMA-associated reduction of UBA1 contributes to neuromuscular pathogenesis through disruption of ubiquitin homeostasis and subsequent β-catenin signaling, highlighting ubiquitin homeostasis and β-catenin as potential therapeutic targets for SMA.

Introduction

Proximal spinal muscular atrophy (SMA) is the leading genetic cause of infant mortality, with a carrier frequency of 1 in 35 in the population of mixed European descent and an incidence of approximately 1 in 6,000–10,000 live births (1, 2). This autosomal recessive neuromuscular disorder is most commonly caused by homozygous deletion of the survival motor neuron 1 (*SMN1*) gene, leading to reduced levels of ubiquitously expressed full-length SMN protein (1, 3). SMA is primarily characterized by degeneration of lower motor neurons and atrophy of skeletal muscle (3, 4), with functional and structural

disruption of synaptic connectivity at neuromuscular junctions (NMJ) and in the spinal cord occurring during the early stages of disease pathogenesis (5–9). However, recent studies have revealed that SMA, particularly in its most severe forms, is a multisystem disorder (10), with other regions of the nervous system also being affected (e.g., the hippocampus; ref. 11) as well as nonneuronal tissues and organs, including heart (12), vasculature (13), liver (14), pancreas (15), lung, and intestines (16). This suggests that SMN deficiency causes perturbations across a wide range of cells and tissues in SMA, albeit with motor neurons being the most vulnerable cell type.

Despite a clear understanding of the genetic causes of SMA, the mechanisms linking low levels of SMN to disease pathogenesis remain unclear. SMN protein is known to play key roles in several core canonical cellular pathways, including snRNP biogenesis and pre-mRNA splicing (3). However, attempts to link disruptions in RNA processing directly to SMA pathogenesis have proven controversial (17–20). The finding that mutations in genes encoding

Table 1

Clustering analysis of proteomics data revealing functional pathways modified in P1 SMA mouse synapses

Pathway	P value	Individual proteins (>20% changed in SMA)
Oxidative phosphorylation	1.61×10^{-07}	ATP5A1, ATP5F1, ATP6V1A, COX5A, CYC1, PPA1
Protein ubiquitination	8.59×10^{-06}	HSP90AA1, HSP90AB1, HSPA9, HSPD1, PSMD2, UBA1, UCHL1
Glycolysis/gluconeogenesis	1.14×10^{-04}	ALDOA, PGAM1, PGK1, PKM2
Purine metabolism	1.15×10^{-04}	ATP1B1, ATP5A1, ATP5F1, HSP90AA1, HSPD1, PKM2
PI3K/AKT signaling	3.64×10^{-04}	CTNNB1, HSP90AA1, HSP90AB1, YWHAG

proteins not directly involved in RNA processing can cause related diseases (e.g., mutations in *BICD2* cause congenital autosomal-dominant SMA, ref. 21; and mutations in ubiquitin-like modifier activating enzyme 1 [*UBA1*] cause X-linked infantile SMA, ref. 22), alongside reports linking SMN protein to actin dynamics (23, 24), Phosphatase and tensin homolog–mediated (PTEN-mediated) protein synthesis pathways (25), and translational regulation (26), suggests that SMN may fulfil additional roles downstream from, or outside of, RNA processing pathways in the nucleus and cell body of neurons. The identification of key pathways downstream from SMN that are critical for the regulation of neuromuscular and system-wide pathology in SMA will be important for designing, testing, and evaluating new therapeutic approaches for SMA patients.

The studies described here were initiated to identify key molecular pathways present in the neuronal cytoplasm and acting downstream of SMN that are responsible for regulating neuromuscular and systemic pathology in SMA. Combining proteomic screens with cellular and molecular approaches in mouse, *Drosophila*, and zebrafish models, we reveal widespread disruption to ubiquitin homeostasis in SMA, leading to perturbations in β-catenin signaling pathways in the neuromuscular system.

Results

Widespread perturbations in ubiquitin homeostasis in animal models of SMA. The initial aim of the study was to identify functional molecular pathways modified downstream of SMN depletion in SMA. In order to examine neuronal material that was biologically relevant and yet free from contamination by nuclear and/or myelin proteins (the abundance of which can hamper the sensitivity of proteomics screens), we initially performed unbiased iTRAQ comparative proteomics on synapses isolated from the hippocampus of presymptomatic (P1) "severe" SMA mice ($Smn^{-/-} SMN2^{tg/tg}$) compared with littermate controls ($Smn^{+/+} SMN2^{tg/tg}$). We chose to use hippocampal synaptosomes for these experiments due to the known susceptibility of the hippocampus in mouse models of SMA (11), as well as the known susceptibility of synaptic compartments of neurons in SMA during the early stages of disease (7, 8). Biochemical analysis of isolated synaptic preparations from mice confirmed the presence of SMN protein and its known interacting proteins (e.g., gemin5) in the synaptic cytoplasm at CNS synapses (Supplemental Figures 1 and 2; supplemental material available online with this article; doi:10.1172/JCI71318DS1). SMN protein was also present in synaptic boutons at the *Drosophila* NMJ (Supplemental Figures 1 and 2), confirming the biological relevance of using synaptic preparations for the initial proteomics screen.

The iTRAQ screen revealed robust disruption of the synaptic proteome in SMA mice, where 52 out of 150 (35%) unique proteins identified had expression levels modified by more than 20%

in SMA mice (Supplemental Tables 1 and 2). Functional clustering analyses, using IPA software (see Methods), linked these individual protein changes to significant modifications in a range of canonical functional pathways (Table 1). Interestingly, these analyses highlighted significant disruption to protein ubiquitination pathways in SMA mice, with decreased levels of UBA1 (Supplemental Figure 3A) and increased levels of ubiquitin carboxyterminal esterase L1 (UCHL1) (Table 1 and Supplemental Tables 1 and 2). Ubiquitination pathways, and UBA1 in particular, were of interest in the context of SMA because mutations in the gene coding for human *UBA1* (*UBE1*) are sufficient to cause a genetically distinct form of the disease, known as X-linked infantile SMA (22). Moreover, ubiquitination pathways are known to regulate axonal and synaptic stability (27) as well as the stability and degradation of the SMN protein itself (28–30).

To establish whether disruption of ubiquitin-dependent pathways was conserved across the range of cells and tissues present in the neuromuscular system, UBA1 protein levels were examined in preparations of spinal cord (Figure 1, A and B, and Supplemental Figure 3B) and skeletal muscle (Figure 1, A and C) from severe SMA mice. UBA1 protein levels were reduced approximately 50% in SMA mouse spinal cord (Figure 1B) and more than 60% in skeletal muscle (gastrocnemius; Figure 1C) at P5.

UBA1 regulates the first stages of an enzymatic cascade in which ubiquitin molecules are ultimately conjugated to target proteins; therefore, disruption of UBA1 (alongside concomitant changes in other ubiquitin-related proteins such as UCHL1) would be predicted to affect overall ubiquitin homeostasis. To determine whether this occurred in SMA, we measured levels of ubiquitin in the spinal cords from severe SMA mice. Levels of both monomeric and multimeric ubiquitin were significantly decreased (Figure 1, D–F). SMN-dependent perturbations in ubiquitin homeostasis were also conserved across other species and tissues, as a dramatic redistribution of mono- and polyubiquitinated proteins was observed in striated muscle from an established *Drosophila* model of SMA (Figure 1G and ref. 31).

To determine the time course of UBA1 changes in SMA, we examined UBA1 expression in "Taiwanese" SMA mice, which display a milder phenotype than severe SMA mice (mean survival of ~11 days compared with ~5–6 days; ref. 32). We examined UBA1 protein expression in motor neuron cell soma located in the ventral horn of spinal cord at presymptomatic (P3) and early symptomatic (P7) stages of disease (Figure 1, H–J). In control mice, UBA1 was almost exclusively localized to the neuronal cytoplasm at P3, before undergoing a dramatic subcellular relocalization to the nucleus by P7 (Figure 1, H and I). There was no overt difference in UBA1 localization in SMA mice at P3. However, at P7, we noted an almost complete absence of UBA1 from the motor neu-
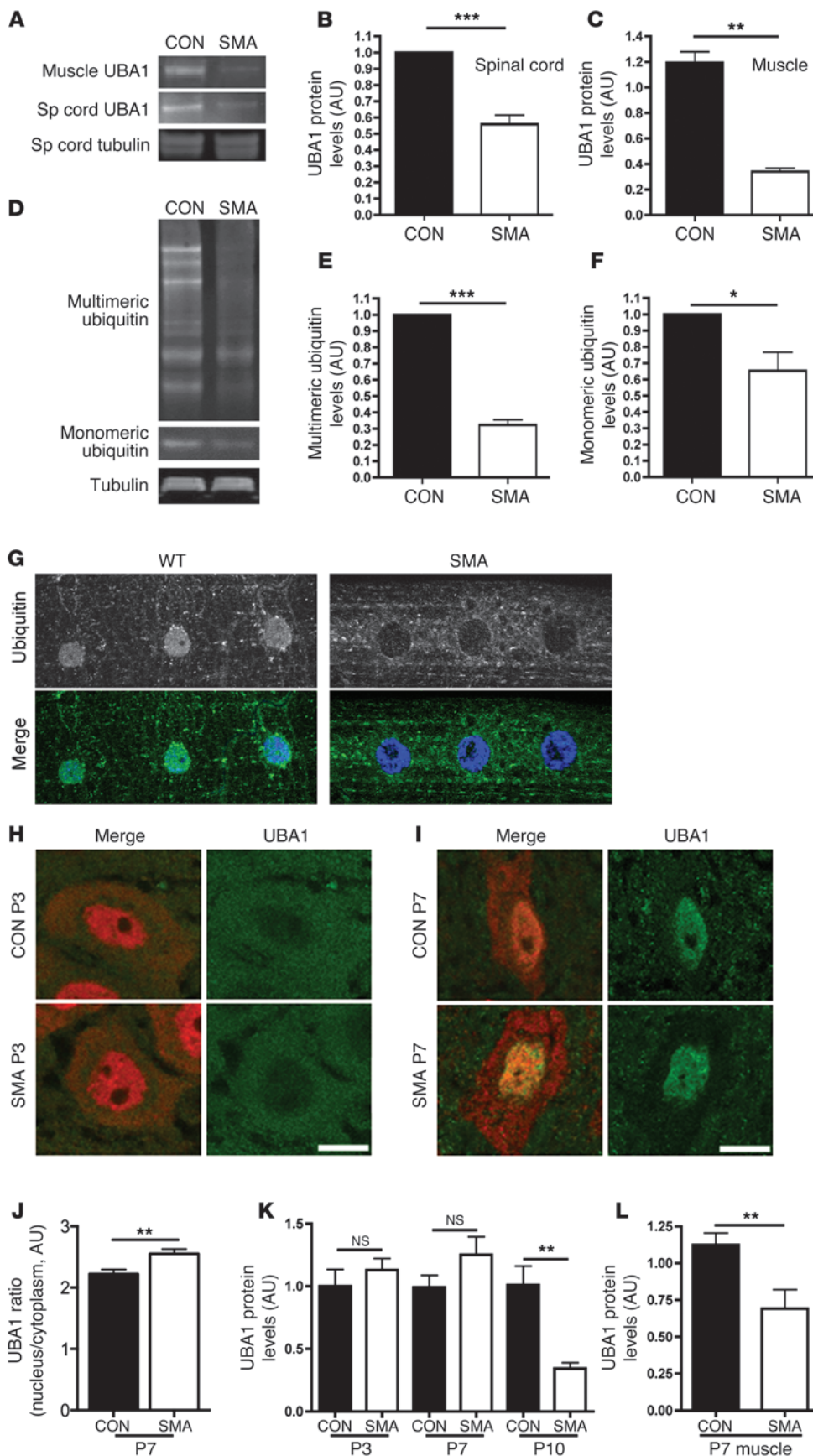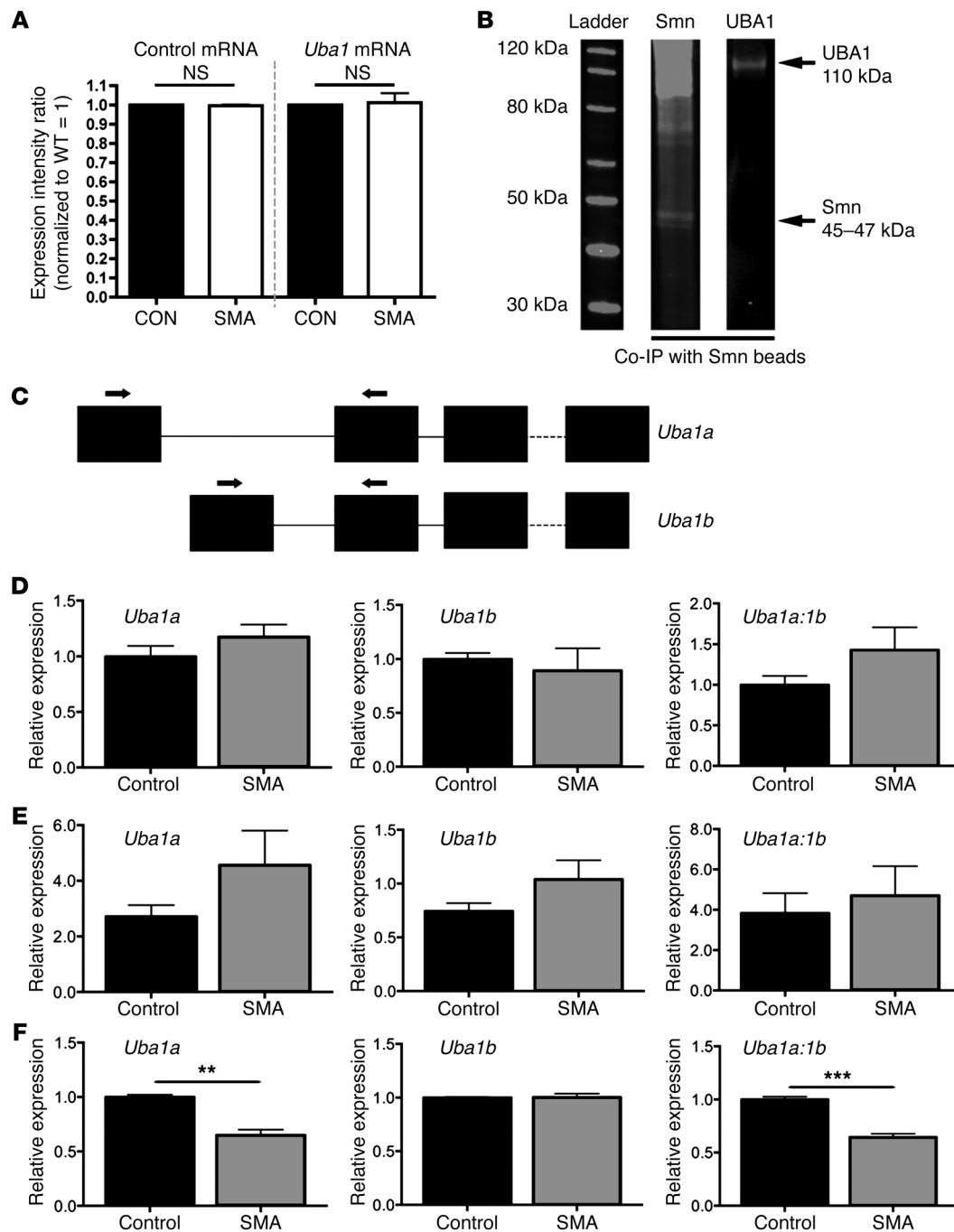
Figure 1
Perturbations in UBA1 levels and ubiquitin homeostasis in mouse and *Drosophila* models of SMA. (**A**–**C**) Significant reduction in levels of UBA1 protein in spinal cord and skeletal muscle from severe SMA mice at P5 compared with littermate controls (con), quantified using fluorescent Western blot ($n = 3$ mice/genotype; unpaired 2-tailed t test). (**D**–**F**) Reduced levels of both monomeric and multimeric ubiquitin in the spinal cord of Taiwanese SMA mice at P10 (tubulin: loading control; $n = 3$ mice/genotype). (**G**) Representative confocal micrographs of striated muscle from WT and SMA *Drosophila* larvae immunolabeled with an antibody that recognizes mono- and polyubiquitinated proteins (green). Diffuse staining in muscle and muscle nuclei (stained with Hoechst, blue) of WT flies contrasted with a distinct lack of nuclear staining and increased perinuclear staining in SMA flies. Each panel in **G** is 75 μm in length. (**H** and **I**) UBA1 (green) and NeuN (red) immunolabeling of motor neurons from Taiwanese SMA and littermate control mouse spinal cords at P3 (**H**) and P7 (**I**). Note how UBA1 was predominantly cytoplasmic at P3 but nuclear at P7. Scale bars: 10 μm. (**J**) Significant increase in the ratio of nuclear to cytoplasmic UBA1 in SMA motor neurons at P7 compared with littermate controls ($n = 24$ motor neurons per genotype). (**K**) UBA1 levels in whole spinal cord of Taiwanese SMA mice remained unchanged at P3 and P7, but were significantly reduced by P10 ($n > 3$ mice per time point/genotype; ANOVA with Tukey's post-hoc test). (**L**) Levels of UBA1 in skeletal muscle were significantly reduced at an early symptomatic age (P7) in Taiwanese SMA mice ($n = 4$ mice per genotype). *$P < 0.05$; **$P < 0.01$; ***$P < 0.001$.

Figure 2

UBA1 physically interacts with SMN protein in vivo, and *Uba1* splicing is dysregulated at late symptomatic time points in SMA mouse spinal cord. (**A**) No change in levels of *Uba1* mRNA (or a control mRNA, *Fth1*; similar control data using *Mapt* not shown) in the spinal cord of P5 severe SMA mice, quantified using qPCR ($n = 3$ mice per genotype; ANOVA with Tukey's post hoc test). (**B**) Representative fluorescent Western blots for SMN (left lane) and UBA1 (right lane) from co-IP experiments on spinal cord extracts from WT mice, using SMN-bound beads, demonstrating that UBA1 physically interacts with SMN in vivo. (**C**) Graphic overview of the exon structure of *Uba1*. Two *Uba1* splice variants are generated with unique first exons. The position of primers used to amplify each splice variant is highlighted. Note that the coding sequence of *Uba1* starts in exon 2. (**D**–**F**) Bar charts showing relative expression levels of *Uba1a* and *Uba1b*, as well as the ratio of *Uba1a* to *Uba1b*, in SMA (Taiwanese) and control spinal cord at P3 (**D**; presymptomatic), P7 (**E**; early symptomatic), and P11 (late-symptomatic) ($n = 3$ mice per genotype, 3 independent amplifications per sample; 2-tailed, unpaired *t* tests). *Uba1* splicing was significantly dysregulated in the late-symptomatic mice. **$P < 0.01$; ***$P < 0.001$.
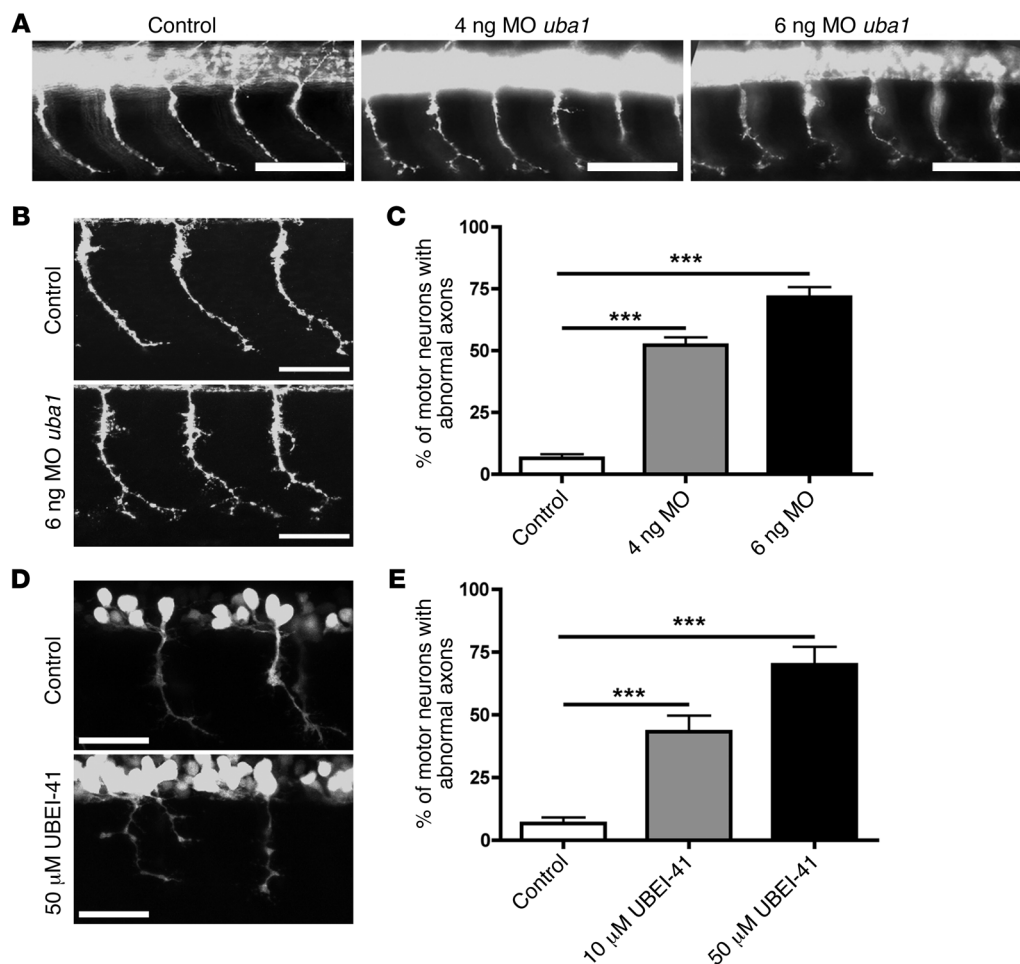
Figure 3
Genetic and pharmacological suppression of *uba1* in zebrafish leads to dose-dependent motor axon pathology. (**A**) Representative fluorescence micrographs of motor axons growing out from the spinal cord in a control zebrafish 34 hours after fertilization, and in animals injected with either 4 ng or 6 ng of a MO suppressing *uba1* levels (see Supplemental Figure 4). (**B**) Representative higher-magnification confocal micrographs showing abnormal sprouts and axonal extensions in motor axons from MO-treated zebrafish. Scale bars: 50 μm. (**C**) Dose-dependent increase in the occurrence of abnormal branching in MO-treated zebrafish (Kruskal-Wallis test with Dunn's post hoc test; uninjected, $n = 310$ motor neurons, $n = 31$ animals; 4 ng, $n = 360$, $n = 36$ animals; 6 ng, $n = 360$, $n = 36$ animals). Only motor axons with modest (type 2; see Supplemental Figure 4) or severely abnormal branching (type 3; see Supplemental Figure 4) were quantified as having abnormal branching. (**D**) Representative confocal micrographs showing perturbations in motor axon morphology in *Tg(hb9:gfp)* zebrafish embryos treated with 50 μM of the UBA1 inhibitor UBEI-41. Note the presence of a "double-exit" motor axon (right hand side of image) in the UBEI-41 example, with the axon branch emerging on the right side of the pair showing stunted outgrowth. Scale bars: 100 μm; 30 μm (**B**, **D**). (**E**) Levels of abnormal motor axon branching and axon outgrowth in UBEI-41–treated zebrafish. Note the dose-dependent increase of numbers of aberrant motor axons in the UBEI-41 group compared with DMSO controls (10 μM UBEI-41 $n = 258$ nerves, $n = 11$ animals; 50 μM UBEI-41 $n = 280$ nerves $n = 12$ animals; Kruskal-Wallis test with Dunn's post hoc test). ***$P < 0.001$.

ron cytoplasm in SMA mice, when low levels persisted in littermate control mice (Figure 1I). Quantification of the ratio of nuclear/cytoplasmic UBA1 levels in SMA mice revealed a significant reduction in the cytoplasm compared with controls (Figure 1J). Thus, redistribution of UBA1 occurring during the early postnatal period was perturbed in SMA mice at early symptomatic stages of the disease. Interestingly, quantification of total UBA1 levels in spinal cord did not reveal a significant reduction in SMA mice until late-symptomatic stages (P10; Figure 1K), suggesting that subtle changes in the subcellular distribution of UBA1 were perturbed in motor neurons in advance of a widespread reduction in protein levels throughout the spinal cord. Comparable examination

of UBA1 levels in whole muscle showed a significant loss by P7 in SMA (Figure 1L), suggesting that muscle may be more severely affected than spinal cord.

SMN-Uba1 interactions and dysregulation of Uba1 splicing in SMA. To investigate potential pathways through which UBA1 and ubiquitin homeostasis are targeted in SMA, we first asked whether changes were occurring due to reduced expression of *Uba1* mRNA. As mRNA levels for *Uba1* remained unchanged in the spinal cords of SMA mice (Figure 2A), it was unlikely that UBA1 protein levels were reduced as a result of global deficiencies in transcription of *Uba1* mRNA. Given that SMN protein interacts with other proteins in vitro, including members of the ubiquitin-proteasome sys-

tem such as UCHL1 (29, 30), we next wanted to determine whether SMN could be influencing UBA1 levels as a result of direct physical interactions in vivo. We therefore performed coimmunoprecipitation (co-IP) experiments on spinal cord extracts from WT mice, using anti-SMN beads. Immunoblotting on the bound extract with antibodies against UBA1 revealed that UBA1 and SMN physically interact in the neuronal cytoplasm in vivo (Figure 2B).

Several recent studies have also implicated SMN in the regulation of splicing; therefore, we next analyzed splicing patterns for *Uba1* in the spinal cords of Taiwanese SMA mice at presymptomatic (P3), early symptomatic (P7), and late-symptomatic (P10) time points (Figure 2, C–F). Two *Uba1* splice variants are generated with unique first exons *Uba1a* and *Uba1b* (Figure 2C). Quantification of relative expression levels of *Uba1a* and *Uba1b* in SMA and control spinal cords at P3 and P7 showed no significant differences between the genotypes (Figure 2, D and E). In contrast, there was a significant reduction in relative expression levels of *Uba1a* (but not *Uba1b*) and a significant alteration in the ratio of *Uba1a* to *Uba1b* in SMA mice at P10 (Figure 2F). Thus, dysregulation of *Uba1* splicing may contribute to the alterations in UBA1 protein levels observed in SMA, with the disruption in splicing in spinal cord temporally correlating with the reduction in UBA1 protein levels in spinal cord (see Figure 1K). Taken together with data showing UBA1 subcellular redistribution and Uba1-SMN interaction, these findings suggest that SMN-dependent regulation of UBA1 and its disruption in SMA is a complex process, with combinatorial effects of disruption to multiple regulatory pathways likely to be responsible.

Suppression of UBA1 is sufficient to induce motor neuron pathology in vivo. Although suppression of UBA1 and disruption of ubiquitin homeostasis were robust correlates of neuromuscular pathology in SMA, it remained unclear whether these changes directly contributed to disease pathogenesis. To examine this possibility, we designed experiments to suppress *uba1* in zebrafish, an accessible model system to assess the effects of genetic manipulations on motor neuron stability (23, 33). Uba1 expression was targeted using an antisense Morpholino oligonucleotide (MO) designed against the translational start codon of the *uba1* gene. Embryos were injected with either 4 ng or 6 ng of MO and examined 34 hours after fertilization. Levels of UBA1 protein were robustly reduced in fish treated at both doses (Supplemental Figure 4A). Suppression of *uba1* using MO had no effect on the gross development of motor neurons in the spinal cord (Figure 3A). However, *uba1* suppression did lead to a profound, dose-dependent disruption of motor axon outgrowth and branching. Whereas the vast majority of axons in control animals showed a simple, unbranched morphology, axons in both 4 ng and 6 ng MO–injected animals revealed grossly abnormal branching patterns (Figure 3, A and B). The percentage of motor axons with branching abnormalities (see Supplemental Figure 4B) increased from less than 5% in controls to approximately 50% in 4 ng MO animals and approximately 75% in 6 ng MO animals (Figure 3C). Importantly, these findings phenocopied branching defects previously reported in zebrafish models of SMA (23, 33).

To confirm these findings using pharmacological suppression of UBA1, we treated zebrafish with UBEI-41, a cell-permeable pharmacological UBA1 inhibitor (34). Inhibition of UBA1 revealed a similar, dose-dependent disruption of motor axon branching (Figure 3, D and E). At a dose of 10 µM UBEI-41, the majority of motor nerve abnormalities were due to aberrant axonal branching

(data not shown). At 50 µM, however, approximately half of the motor nerve abnormalities observed (47.2%) were a result of aberrant nerve branching, with the remaining motor nerves revealing a more severe phenotype: truncated or missing motor axons (Figure 3D). Once again, these pathological events phenocopied motor axon defects observed in zebrafish models of SMA (23, 33). Thus, suppression of *uba1* was sufficient to phenocopy SMA-like motor neuron pathology in vivo. In addition to the observed motor axon defects, *uba1* suppression led to body axis defects in zebrafish, both following UBEI-41 treatment and following MO treatment (data not shown). However, the viability of the fish was not compromised, as there was not a significant increase in the number of fish dying after *uba1* suppression.

SMN-dependent suppression of UBA1 leads to accumulation of β-catenin. Given that UBA1 is a key component of ubiquitination pathways through which substrate proteins are "tagged" for targeting to the proteasome, we therefore wanted to identify specific substrate proteins affected as a downstream consequence of the disruption to ubiquitin homeostasis in SMA. Perturbations in ubiquitin pathways are often associated with a failure to degrade target proteins, resulting in a characteristic accumulation within the cell. Reexamination of our original proteomics data set revealed that β-catenin levels were robustly increased, by more than 400%, in SMA mice (Table 1 and Supplemental Tables 1 and 2). Examination of β-catenin levels in freshly prepared synaptosomes from control ($Smn^{+/+}$ $SMN2^{tg/tg}$), heterozygous ($Smn^{-/+}$ $SMN2^{tg/tg}$) and homozygous ($Smn^{-/-}$ $SMN2^{tg/tg}$) severe SMA mice confirmed that increased levels of β-catenin corresponded to reduced levels of SMN protein in a dose-dependent manner (Figure 4A). β-catenin levels were also significantly increased in the spinal cords of Taiwanese SMA mice (Figure 4B and Supplemental Figure 6). Alongside changes in β-catenin levels, levels of stabilized β-catenin (ABC) were reduced in the spinal cord (Figure 4C and Supplemental Figure 5), and levels of transcription factor 4 (TCF-4), a key β-catenin–interacting protein required for activation of downstream response genes (35), were also significantly reduced (Figure 4D and Supplemental Figure 5). Importantly, β-catenin protein levels in muscle biopsy samples from SMA patients suggested that elevated levels were also a major feature of neuromuscular pathology in human patients (Figure 4I).

To confirm that increased levels of β-catenin were occurring downstream of perturbations in UBA1, we examined global β-catenin levels in zebrafish treated with 4 ng or 6 ng MO against *uba1*. β-Catenin levels were increased in a dose-dependent manner, reaching approximately 250% of control levels in zebrafish treated with 6 ng MO against *uba1* (Figure 4E). To further confirm a link between UBA1 levels and the regulation of β-catenin in neurons, cultures of primary hippocampal neurons and NSC-34 motor neuron–like cells (36) were exposed to the UBA1 inhibitor UBEI-41 for 2 hours. UBEI-41 treatment led to a rapid and significant increase in levels of β-catenin in hippocampal neurons (~50%; Figure 4F), with an even more robust increase in β-catenin levels observed in NSC-34 cells (~90%; Figure 4F), suggesting that motor neurons were particularly susceptible to suppression of UBA1. To establish whether increased levels of β-catenin protein led to a corresponding increase in β-catenin signaling activity, we performed luciferase activity reporter experiments. β-Catenin activity was significantly increased in NSC-34 cells treated with UBEI-41 for 2 hours (Figure 4G). In order to ascertain whether such changes in β-catenin signaling activity could explain changes
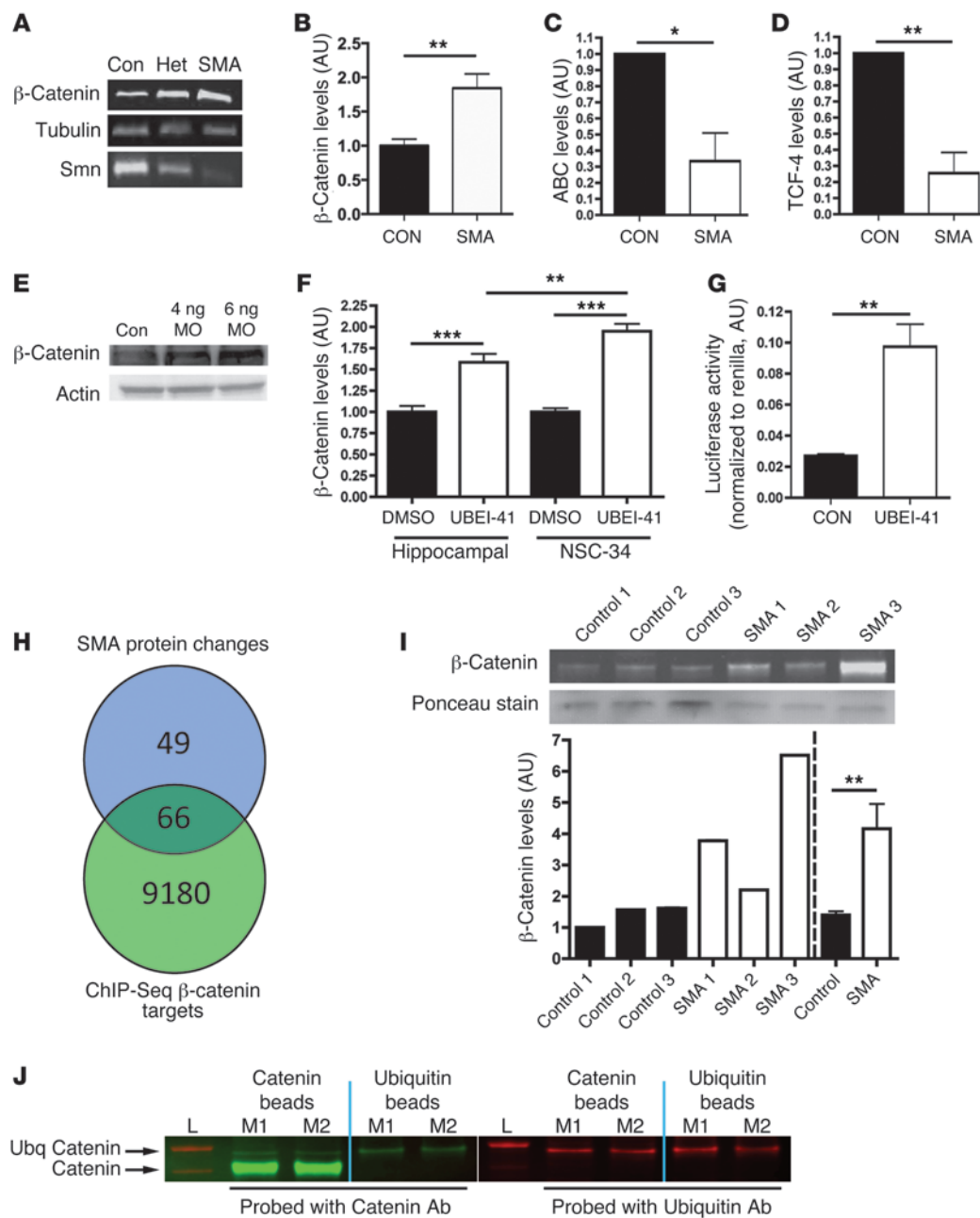
Figure 4

β-Catenin is a downstream target of UBA1 and accumulates in SMA. (**A**) β-Catenin and SMN protein in spinal cord of severe SMA, heterozygous (Het), and littermate (con) mice at P5 (tubulin: loading control). (**B–D**) β-Catenin was increased in P10 Taiwanese SMA mouse spinal cord ($n = 3$ control mice, $n = 4$ SMA; unpaired 2-tailed t test), whereas stabilized β-catenin (ABC; **C**) and TCF-4, a β-catenin interacting protein required for activation (**D**), were both reduced ($n = 3$ CON, $n = 3$ SMA). (**E**) Increased β-catenin protein in zebrafish injected with 4 ng or 6 ng of a *uba1* MO 48 hours after fertilization. (**F**) Increased β-catenin in rat hippocampal neurons and a motor neuron cell line (NSC-34) treated with 50 μM UBEI-41 (ANOVA with Tukey's post-hoc test; $n = 12$ coverslips DMSO, $n = 15$ UBEI-41 hippocampal; $n = 19$ DMSO, $n = 18$ UBEI-41 NSC-34). (**G**) Increased β-catenin signaling activity in NSC-34 cells treated with 50 μM UBEI-41 measured with a luciferase reporter construct ($n = 3$ coverslips per treatment). (**H**) The majority of proteins modified in SMA synapses (66 out of 115 analyzed; see Supplemental Tables 1 and 2) are known β-catenin target genes identified by ChIP-Seq analyses. (**I**) Increased β-catenin protein in muscle biopsies from 3 human SMA patients (pooled data on right of dotted line). (**J**) Western blots for β-catenin (left panel; green) and ubiquitin (right panel; red) from co-IP experiments on synaptic extracts from 2 WT mice (L, ladder; M1, mouse 1; M2, mouse 2). Immunoblotting on the bound extract revealed the presence of ubiquitinated β-catenin (upper arrow). *$P < 0.05$; **$P < 0.01$; ***$P < 0.001$.

research article
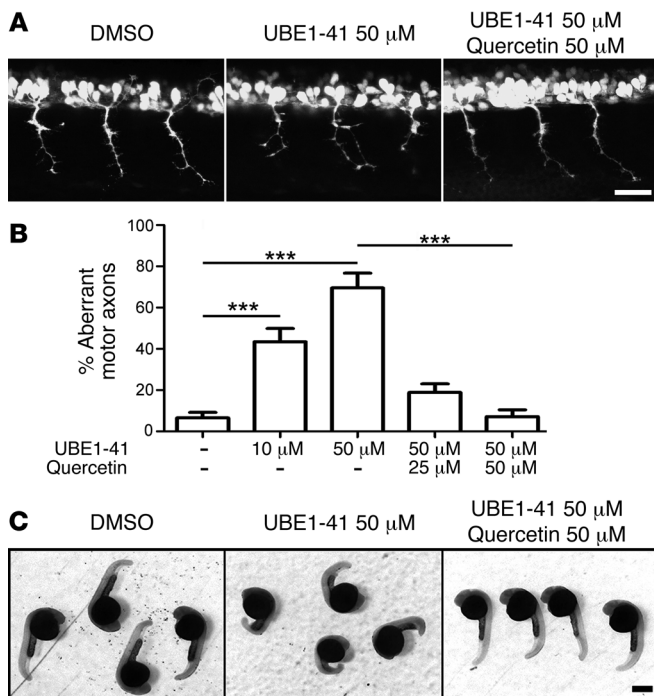
Figure 5
Rescue of *uba1*-dependent motor axon defects in zebrafish by pharmacological inhibition of β-catenin signaling. (**A**) Representative confocal micrographs showing 3 segments of *Tg(hb9:gfp)* zebrafish embryos from the trunk region. Note the severe branching phenotype of the motor nerves in the UBEI-41–treated animal. This phenotype was rescued by quercetin treatment. Scale bar: 30 μm. (**B**) Dose-dependent increase in numbers of aberrant motor axons in the UBEI-41–treated group compared with DMSO controls. This phenotype was rescued by quercetin in a dose-dependent manner (DMSO controls: *n* = 331 nerves, *n* = 14 animals; 10 μM UBEI-41: *n* = 258, *n* = 11; 50 μM UBEI-41 *n* = 280, *n* = 12; 50 μM UBEI-41 + 25 μM quercetin: *n* = 143, *n* = 6; 50 μM UBEI-41 + 50 μM quercetin: *n* = 168, *n* = 7; Kruskal-Wallis test with Dunn's post hoc test). (**C**) Representative overview images showing body axis defects in zebrafish embryos after UBEI-41 treatment compared with DMSO controls. Note the rescue of this gross phenotype following application of 50 μM quercetin. ***$P < 0.001$.

in levels of other proteins found to be altered in SMA synaptosomes, we compared our proteomics data set to published β-catenin ChIP-Seq data revealing potential downstream targets of β-catenin (37). This analysis revealed that the majority of proteins modified in SMA synapses (66 out of 115 analyzed) were also present in the ChIP-seq data (Figure 4H), indicative of them being putative β-catenin targets.

β-catenin is a known target of the ubiquitin-proteasome system (38), but we wanted to confirm that β-catenin was being ubiquitinated in neurons. We therefore performed IP experiments on protein isolated from synaptosomes generated from WT mice (as in our initial proteomics screen, where increased levels of β-catenin were identified) using either β-catenin beads or pan-ubiquitin beads. Western blotting with antibodies against β-catenin and ubiquitin demonstrated that ubiquitinated forms of β-catenin were present in neurons and their synaptic compartments (Figure 4J).

Inhibition of β-catenin signaling reverses UBA1-dependent destabilization of motor neurons. To test whether the UBA1-dependent effects on motor nerve branching we observed previously were mediated by downstream effects on β-catenin signaling pathways, we exposed zebrafish embryos treated with the UBA1 inhibitor UBEI-41 to quercetin, a plant-derived flavonoid that robustly inhibits β-catenin signaling pathways by disrupting transcriptional activity of the β-catenin–Tcf complex (39–41). Treatment of fish with motor neuron defects resulting from the addition of 50 μM UBEI-41 with 25 μM or 50 μM quercetin revealed a dose-dependent rescue of the motor axon branching phenotype (Figure 5, A and B). Strikingly, in the fish treated with 50 μM quercetin, the number of abnormal motor nerves was reduced to that observed in control fish not exposed to the UBA1 inhibitor. Treatment with 50 μM quercetin also ameliorated motor axon branching defects in zebrafish treated with MO against *uba1* (data not shown). Thus, motor nerve abnormalities induced by inhibition of *uba1* in zebrafish were fully rescued by simultaneous inhibition of β-catenin sig-

naling. In addition to the motor nerve disruptions observed, we noted that exposure to UBEI-41 caused dose-dependent alteration of the gross morphology of zebrafish embryos, manifesting as a bent body axis (Figure 5C). These deficits were also corrected by treatment with quercetin (Figure 5C).

Inhibition of β-catenin signaling ameliorates neuromuscular pathology in zebrafish and Drosophila models of SMA. Given that pharmacological inhibition of β-catenin signaling with quercetin was sufficient to block motor axon defects resulting from targeting of UBA1, we next wanted to know whether pharmacological inhibition of β-catenin signaling would have similar beneficial effects on neuromuscular pathology in animal models of SMA. Treatment with 50 μM quercetin robustly and significantly reduced the incidence of both truncated motor axons and motor axon branching defects in SMA zebrafish (33), reducing levels of motor axon pathology back to those observed in healthy control animals (Figure 6, A–C). Similarly, quercetin treatment reversed morphological defects associated with the NMJ in a dose-dependent manner in an established *Drosophila* model of SMA (31), rescuing both synaptic bouton size and bouton density in the treated SMA flies (Figure 6, D–F). Thus, pharmacological inhibition of β-catenin signaling with quercetin ameliorated key markers of neuromuscular pathology in both invertebrate and vertebrate models of SMA.

Inhibition of β-catenin signaling ameliorates neuromuscular pathology, but not systemic pathology in SMA mice. Finally, we wanted to establish whether pharmacological inhibition of β-catenin signaling with quercetin could have a similar effect on disease phenotype in SMA mice. Taiwanese SMA mice and littermate controls were treated with 10 mg/kg quercetin daily (i.p. injection) from birth. A parallel group of mice received injections of DMSO vehicle only. Treatment with 10 mg/kg quercetin was well tolerated by healthy littermate controls (an increased dose of 50 mg/kg quercetin was found to have toxic effects after several days of administration) and had no significant detrimental effect on neuromuscular function in SMA mice at presymptomatic ages (P3; Figure 7A). In contrast, quercetin treatment significantly improved the performance of early and late-symptomatic SMA mice on the righting test (Figure 7A). Quercetin treatment ameliorated motor neuron cell body loss from the spinal cord (Figure 7, B and C), restored muscle fiber diameters of SMA mice to those of littermate control mice at late-symptomatic stages (P11; Figure 7, E and F), and also ameliorated NMJ pathology, restoring the average number of axonal inputs in SMA mice to the same levels observed in littermate controls
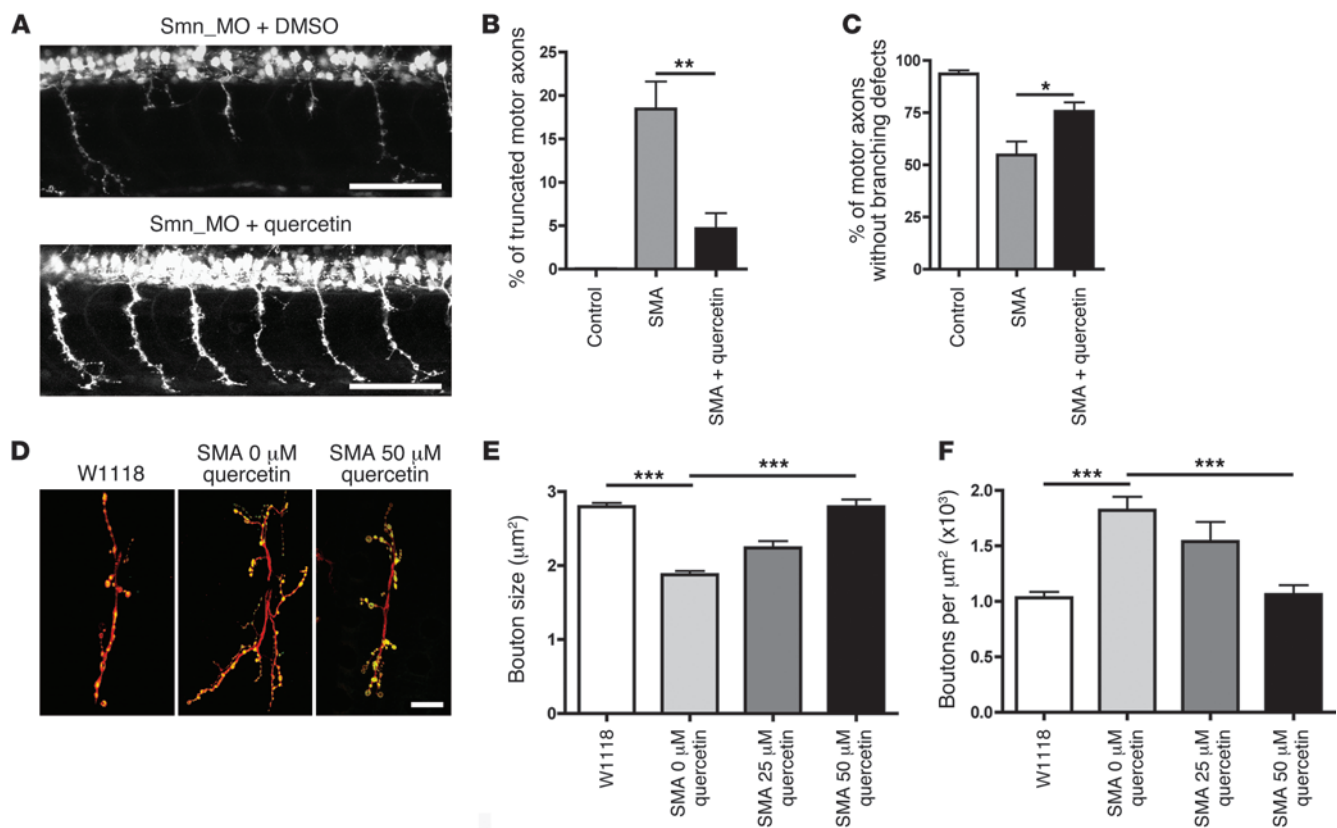
Figure 6
Amelioration of neuromuscular pathology in zebrafish and *Drosophila* models of SMA following pharmacological inhibition of β-catenin signaling. (**A**) Representative confocal micrographs of motor axons growing out from the spinal cord in a SMA zebrafish 34 hours after fertilization (top panel) as well as an SMA zebrafish treated with 50 μM quercetin (bottom panel). Note the abnormal outgrowth and branching of motor axons in SMA zebrafish absent in the SMA zebrafish treated with quercetin. Scale bar: 100 μm. (**B** and **C**) Significant improvement in the number of truncated motor axons (**B**) and abnormally branched motor axons (**C**) in SMA zebrafish treated with 50 μM quercetin (Kruskal-Wallis test with Dunn's post hoc test; $n = 31$ animals, control; $n = 32$ SMA; $n = 30$ SMA + 50 μM quercetin). (**D**) Representative confocal micrographs of NMJs in WT *Drosophila* (w[1118]), SMA *Drosophila* without quercetin, and SMA *Drosophila* fed 50 μM quercetin. NMJs were stained with anti-HRP to visualize axons and anticysteine string protein to identify synaptic boutons. Scale bar: 10 μm. (**E** and **F**) Feeding SMA *Drosophila* 50 μM quercetin restored bouton size (**E**) and rescued synaptic overgrowth (**F**) ($n = 8$ larvae per treatment; ANOVA with Tukey's post test). *$P < 0.05$; **$P < 0.01$; ***$P < 0.001$.

(Figure 7, G and H). Thus, as we previously observed in zebrafish and *Drosophila* models, pharmacological inhibition of β-catenin signaling with quercetin ameliorates neuromuscular dysfunction and pathology in SMA mice.

Quercetin-treated mice often appeared much healthier than their DMSO-treated counterparts at late symptomatic stages (Figure 7D), but treatment with quercetin did not increase survival (Figure 7I) or average body weight (Supplemental Figure 6). Examination of quercetin-treated mice postmortem revealed the presence of widespread gross organ defects previously reported in SMA mice (Figure 7J), where systemic pathology is known to target organs including the heart and liver (10, 14, 16). In order to examine the possible causes of this failure to ameliorate nonneuromuscular, systemic pathology (even when quercetin was administered systemically via i.p. injection), we quantified UBA1 and β-catenin levels in the heart and liver from late-symptomatic Taiwanese SMA mice and littermate controls. Levels of UBA1 in the heart and liver were reduced in SMA mice to a level similar to that observed in spinal cord (Figure 7K). Surprisingly, however, β-catenin levels were not significantly modified in the heart and liver (Figure 7H).

Thus, perturbations in β-catenin signaling pathways occurring downstream of disrupted ubiquitin homeostasis were restricted to the neuromuscular system and were not repeated in nonneuromuscular organs. This suggests that distinct mechanisms drive pathology in the neuromuscular system compared with other tissue and organ systems in SMA and may explain, at least in part, why pharmacological inhibition of β-catenin selectively ameliorated neuromuscular pathology in SMA mice.

Discussion

The studies described here were initiated to identify novel regulators of neuromuscular pathology in SMA. Using rodent, *Drosophila*, and zebrafish SMA models, we have revealed an important role for ubiquitin homeostasis, mediated largely via modifications in levels of UBA1. Suppression of UBA1 in SMA is likely to result from a complex series of events, including disruptions in both splicing of *Uba1* mRNA and physical interactions between SMN and UBA1 protein in the cytoplasm. Experimental downregulation of UBA1 expression was sufficient to generate motor neuron pathology in vivo, phenocopying the severe axonal defects
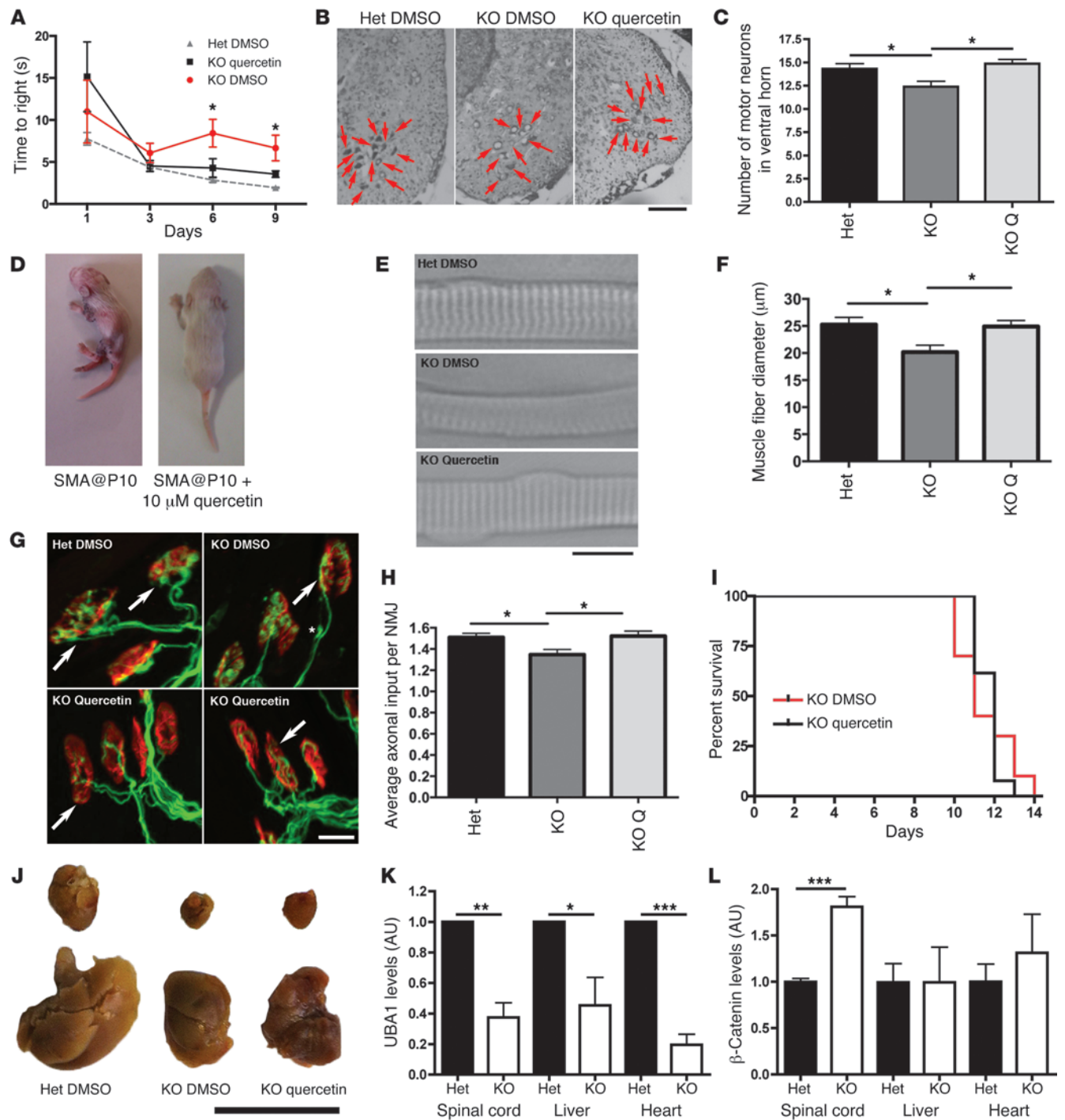
Figure 7

Pharmacological inhibition of β-catenin ameliorates neuromuscular, but not systemic, pathology in SMA mice. (**A**) Significant improvement on the righting test in early (P6) and late-symptomatic (P9) Taiwanese SMA mice (KO) treated with 10 mg/kg quercetin (Kruskal-Wallis test with Dunn's post hoc; P3, $n = 30$ tests Het; $n = 27$ KO; $n = 21$ KOQ; P6, $n = 31$, Het; $n = 28$ KO; $n = 27$ KOQ; P9, $n = 32$, Het; $n = 27$ KO; $n = 36$ KOQ). (**B** and **C**) Reduced motor neuron loss from spinal cord of quercetin-treated SMA mice at P10. (**D**) Untreated (left) and a quercetin-treated (right) SMA mice at P10. (**E** and **F**) Amelioration of skeletal muscle fibre atrophy in the levator auris longus (LAL) muscle of quercetin-treated SMA mice at P10 ($n = 8$ muscles Het, $n = 9$ KO, $n = 4$ KOQ). (**G** and **H**) Reduced NMJ pathology (average number of axonal inputs per NMJ; multiply innervated NMJs are indicated by arrows) in the LAL muscle of quercetin-treated SMA mice at P10 ($n = 8$ muscles Het, $n = 9$ KO, $n = 4$ KOQ). (**I**) Survival curve for quercetin-treated SMA mice showing no significant difference compared with DMSO-treated controls ($P = 0.9897$, χ^2 test; $n = 10$ mice DMSO; $n = 13$ quercetin). (**J**) Hearts (top) and livers (bottom) from control, SMA (KO DMSO), and quercetin-treated SMA (KO quercetin) mice at P10 showing no improvement in gross pathology. (**K** and **L**) UBA1 levels were reduced in all tissues from SMA mice at P10, but β-catenin levels were only correspondingly increased in spinal cord ($n > 3$ mice per genotype; ANOVA with Tukey's post-hoc). Scale bars: 200 μm (**B**), 25 μm (**E** and **G**), 5 mm (**J**). *$P < 0.05$; **$P < 0.01$; ***$P < 0.001$.

previously reported in zebrafish models of SMA (33). We identified β-catenin as a downstream target of UBA1/ubiquitination pathways in the neuromuscular system and showed a robust accumulation of β-catenin in SMA. Pharmacological inhibition of β-catenin signaling using quercetin ameliorated neuromuscular pathology caused by targeting of UBA1 and in zebrafish, *Drosophila*, and mouse models of SMA. Whereas disruption of UBA1 was found to occur across a range of neuronal and nonneuronal organs in SMA mice, surprisingly, we found that downstream disruption of β-catenin was restricted to the neuromuscular system and was not responsible for regulating SMN-dependent pathology in other tissues and organs. Our findings provide experimental evidence directly linking the regulation of ubiquitin homeostasis and β-catenin signaling to neuromuscular pathology in SMA and also reveal fundamental molecular differences between pathways underlying neuromuscular and systemic pathology in SMA.

Although it is known that SMN protein interacts with the ubiquitin-proteasome system in order to regulate its own stability (28–30), our study markedly extends our understanding of the importance of these interactions to include a direct role for dysregulation of ubiquitin homeostasis in the pathogenesis of SMA. When taken together with human genetic data showing that mutations in *UBA1* cause pathological changes similar to those found in SMN-dependent SMA (22), our findings suggest that perturbations in ubiquitin homeostasis, and UBA1 in particular, may represent a common molecular pathway underlying neuromuscular pathology across genetically distinct forms of the disease. Moreover, the finding that perturbations in ubiquitin homeostasis in response to SMN deficiency as well as dysregulation of β-catenin downstream of perturbations in UBA1 are evolutionarily conserved among mouse, zebrafish and *Drosophila* models suggests that regulation of ubiquitin homeostasis represents a core response to low levels of functional SMN protein. Our finding that loss of UBA1 protein in SMA likely resulted from perturbations to both *Uba1* mRNA missplicing and disruption to physical interactions between SMN and UBA1 as well as modifications to normal postnatal subcellular redistribution of the protein suggests that molecular pathways responsible for controlling UBA1 levels in vivo are complex and multifaceted. However, the demonstration of interactions between UBA1 and SMN provides additional evidence to support the hypothesis that interactions between SMN and ubiquitination pathways are key for the normal form and function of the neuromuscular system, not only with regards to the regulation of SMN protein stability (28–30), but also with respect to modulating ubiquitin homeostasis and cell viability.

Our identification of β-catenin as a key downstream target of ubiquitin pathways disrupted in SMA provides mechanistic insights into the pathways through which defects in ubiquitin homeostasis are transferred into pathological changes in the neuromuscular system. Although these pathways have not previously been linked to neuromuscular pathology in SMA, β-catenin signaling pathways are known to play an important role in regulating motor neuron differentiation and stability, including regulating synaptic structure and function (42–44). Interestingly, Li and colleagues previously reported that motor neuron differentiation is regulated by retrograde signaling through β-catenin from skeletal muscle (43). Our demonstration of robust amelioration of neuromuscular pathology in zebrafish, *Drosophila*, and mouse models of SMA treated with quercetin highlights the fact that β-catenin pathways in the neuromuscular system are amenable to pharma-

cological targeting in vivo. It should be noted, however, that quercetin is a pleiotropic flavonoid and as such is capable of modifying targets alongside β-catenin pathways. Nevertheless, targeting β-catenin signaling pathways (in addition to other pathways moderated by quercetin) during the early stages of disease may represent an attractive therapeutic option for stabilizing the neuromuscular system in SMA, and possibly also related conditions.

Given that β-catenin is such a well-established target for the ubiquitin-proteasome system and the magnitude of changes in β-catenin pathways observed in the neuromuscular system in SMA mice, it was surprising to find that quercetin treatment did not target systemic pathology in SMA. However, our finding that β-catenin signaling pathways remained stable in tissues and organs outside the neuromuscular system in SMA mice provides an explanation for this result and serves to highlight an underappreciated complexity in molecular pathways underlying disease pathogenesis in SMA. These findings also add further significant support to the hypothesis that SMA is a multisystem disorder (10) and add an additional layer of complexity with regards to distinct molecular pathways driving pathology in different tissues. Moreover, they further highlight the likely requirement to deliver therapeutics targeting either the *SMN1* or *SMN2* gene systemically in order to fully rescue SMA symptoms (14).

Methods

Mice, human patient samples, and study approvals. Severe ($Smn^{-/-}$ $SMN2^{tg/tg}$; ref. 45) and Taiwanese ($Smn^{-/-}$ $SMN2^{tg/0}$; refs. 32, 46) SMA mice, both on a congenic FVB background, were obtained from Jackson Laboratories and maintained at the University of Edinburgh. Littermate animals either WT or heterozygous for *Smn* ($Smn^{+/+}$ or $Smn^{+/-}$) were used for controls. Mice were bred and sacrificed under license from the United Kingdom Home Office, and were genotyped using standard PCR methods (5, 32).

Skeletal muscle (*quadriceps femoris*) biopsy samples were obtained from 2 different biobanks in Italy (Fondazione IRCCS Istituto Neurologico Carlo Besta, Milan; Fondazione Ospedale Maggiore Policlinico Mangiagalli e Regina Elena, IRCCS, Milan) through EuroBioBank (http://www.eurobiobank.org/). Biopsies were obtained from 3 type II/III SMA patients (aged between 3 and 25 years old), with a confirmed homozygous deletion of the *SMN1* gene confirming a genetic diagnosis of SMA (47). Three age-matched control samples were also obtained; these were genetically confirmed to have no mutations in the *SMN1* gene.

iTRAQ quantitative proteomics. iTRAQ proteomics was performed on freshly isolated synaptosome preparations from the hippocampus of P1 $Smn^{-/-}$ $SMN2^{tg/tg}$ (severe) and $Smn^{+/+}$ $SMN2^{tg/tg}$ (control) mice (n = 9 mice per genotype), as previously described (48). Samples were run in duplicate using the 4-plex system (114 and 116, SMA; 115 and 117, control). Only proteins identified by 2 or more unique peptides were taken forward for subsequent analysis. A stringent cut-off threshold of 20% change (increase or decrease) was used to identify proteins with modified expression. In silico functional pathways analyses were performed using Ingenuity Pathway Analysis software (48).

Western blot analyses. Quantitative Li-Cor fluorescent Western blotting was performed as previously described (4) using the following primary antibodies: SMN, synaptophysin (Santa Cruz Biotechnology Inc.); SMN, β-catenin (BD Biosciences); βIII tubulin, UBA1 (Abcam); histone H2B, active motif; Cox IV (MitoSciences); Ubiquitin (UBI1) (Millipore). Where required, 2 independent sets of measurements were produced per sample in order to minimize the effects of different laser scan intensities on the resulting data (e.g. where strong and weak bands were being measured on the same gel). Standard Western blotting was performed using the fol-

lowing primary antibodies: SMN: all MANSMA antibodies (49); gemin5: GEM5M, GEM5O, GEM5Q. All protein levels reported on graphs represent arbitrary fluorescence units.

IP experiments. IP was performed as previously described (50). Briefly, protein was extracted in NP-40 lysis buffer (Novex; Life Technologies) containing 1% protease inhibitor cocktail (Roche). Following centrifugation at 16000 g, the supernatant was added to Dynabead protein G anti-mouse beads bound with preselected antibodies (β-catenin, UCHL1, and SMN) and subjected to quantitative fluorescent immunoblotting.

For Gemin5 IP experiments, anti-mouse Pan Ig–coated magnetic beads (50 μl) (Dynal) were washed in 4% BSA/PBS and incubated for 30 minutes with a monoclonal SMN antibody (10 μg; MANSMA12), GEM5M antibody against Gemin 5, or 150-kDa neurofilament antibodies as a control. After washing, beads were incubated with synaptosome extract for 1 hour, followed by washing 5 times with PBS. Proteins bound to beads were eluted by boiling in 2× SDS sample buffer, as previously described (51).

RNA extraction, qPCR, and Uba1 splicing assays. mRNA was extracted from synaptosomes using an RNeasy Microkit (QIAGEN). Samples were checked for DNA contamination, and concentration was determined using a nanodrop spectrophotometer (Thermo Scientific). Quantitative RT-PCR (qRT–PCR) was carried out using a SYBR Green 1-step qRT-PCR Kit (Invitrogen) on a Model 7700 instrument (Applied Biosystems). The following primers were used: *Uba1*, forward GAGCGGGGACTTTGTCTCCT; *Uba1*, reverse CTTTGACCTGACTGACGAT; *Fth1*, forward AATTTCTT-GACCCACTGGTGCACT; *Fth1*, reverse TCGAATCGAGAGTAGTGGCA-CA; *Mapt*, forward GATTCTCGTGAGGTTGACGACT; *Mapt*, reverse TAC-GGACGAAGAAGCCGACATT.

mRNA was extracted from spinal cord using an RNeasy Microkit (QIAGEN). Samples were checked for DNA contamination, and concentration was determined using a nanodrop spectrophotometer (Thermo Scientific). RNA integrity was checked visually by resolution on agarose gels. cDNA was made from 2 μg RNA using the High Capacity cDNA Reverse Transcription Kit (Invitrogen). Primers were designed that amplified the 2 mouse Uba1 transcripts, using a unique forward primer with a common reverse primer (*Uba1a*, forward GCTTGTCTCCAGAAGGAAGG; *Uba1b*, forward CTT-GACTTCGGCTCCTTGAG; *Uba1a/Uba1b*, reverse CACTGAGGACACTTC-GGACA). Two mouse housekeeping genes (*GAPDH* and *OAZ1*) were used (*GAPDH*, forward CGTCCCGTAGACAAAATGGT; *GAPDH*, reverse GAATTTGCCGTGAGTGGAGT; *OAZ1*, forward ATCCTCAACAGCCACT-GCTT; *OAZ1*, reverse CGGACCCAGGTTACTACAGC). For real-time detection, an ABI7000 machine (Applied Biosystems) was used. cDNA was amplified using 0.5 to 1 μM primer with the DyNAmo Flash SYBR Green qPCR kit (Thermo Scientific) and using a standard PCR program with amplification at 60°C. Each cDNA sample was amplified in triplicate with all primer pairs. Experimental CT values for each sample were compared, and samples representing CT minimum for each primer pair were identified. The equation where raw data = $1+E^{(Ctmin-Ct)}$ was used to determine relative expression levels for each sample. Raw values obtained for *Uba1a* and *Uba1b* were normalized using the geometric mean of the 2 housekeeping genes.

Drosophila experiments. To examine localization of SMN, pan-neural expression of *UAS-YFP-dSMN* was driven by Elav-Gal4^{C155}. *MHC82-Gal4C* crossed to *UAS-YFP-dSMN* flies were used as controls. Wandering third instar larvae were dissected in PBS and fixed for 10 minutes in 4% paraformaldehyde. GFP staining at NMJs was detected by blocking larval fillets in 3% BSA, 0.1% Triton X-100 in PBS overnight, incubating in primary antibody, 1:400 (chicken anti-GFP; A10262, Invitrogen), followed by secondary antibody, 1:250 (goat anti-chicken Alexa Fluor 488; A11039, Invitrogen). NMJs and motor neurons were visualized with Dylight 649–conjugated anti-HRP, 1:200 (Jackson ImmunoResearch). Images were acquired on a Zeiss LSM510 Meta using a Pan Apochromat 63× 1.4 NA oil immersion objective.

To examine levels of mono- and polyubiquitinated proteins in SMA skeletal muscle, we used wandering third instar larvae null for SMN (31). Ubiquitinated proteins were detected using an anti–mono- and polyubiquitinylated primary antibody (1:100; FK2; BML-PW8110, Enzo Life Sciences). Nuclei were visualized using Hoechst (1:500). For the quercetin rescue experiments, SMN or WT flies (w^{1118}) were maintained on a diet of Drosophila Quick Mix Medium (Blades Biological) containing 0 to 50 μM quercetin hydrate (Sigma-Aldrich). Third instar *smn* null larvae were dissected and fixed. NMJ were visualized using Dylight 649–conjugated anti-HRP (1:200, Jackson ImmunoResearch), and the presynaptic marker cysteine string protein (1:200, Developmental Studies Hybridoma Bank) was used to identify synaptic boutons. The average number of boutons (normalized to muscle area) per NMJ at muscle 6/7 was calculated. Maximum bouton diameters were averaged per NMJ at muscle 6/7.

UBEI-41 in vitro experiments. Primary rat hippocampal cultures were established from E18 Sprague-Dawley rat embryos as previously described (52). NSC-34 cells (36) were generated from existing stocks held at the University of Edinburgh. UBEI-41 (Biogenova), a cell-permeable UBA1 inhibitor with an IC$_{50}$ of approximately 5 μM, was added to the culture medium (50 μM) for 2 hours. β-catenin levels (and β-III tubulin loading control levels) were quantified using fluorescent Western blotting (see above) with anti–β-catenin (1:1000; BD Transduction Laboratories) and anti–β-III tubulin (1:1600; Abcam) primary antibodies.

To quantify β-catenin activity, NSC-34 cells were transiently transfected with a TOPflash reporter plasmid containing a luciferase reporter under the control of 3 copies of the TCF/LEF-binding element upstream of the thymidine kinase minimal reporter, specifically regulated by Wnt/β-catenin signaling. NSC-34 cells were seeded in a 24-well plate, and at 70%–80% confluency, cells were transfected, in triplicate, with 350 ng TOPflash plasmid using Lipofectamine 2000 (Invitrogen). To control for transfection efficiency, 20 ng phTKRenilla luciferase plasmid was used. Cells were treated with 50 μM UBEI-41 28 hours after transfection. Transfected samples were analyzed for firefly and Renilla luciferase activities 30 hours after transfection using the Dual-Luciferase Reporter Assay System (Promega) and measured using a FLUOstar OPTIMA Microplate Reader (BMG LABTECH). All values were corrected to blank wells and normalized to expression from the phTKRenilla plasmid.

Zebrafish uba1 and smn knockdown. An antisense MO was designed against the translational start codon of the *uba1* gene (Gene Tools LLC): 5′-ACAGC-GGCGAGCTGGACATCGTTTC-3′. The previously published smn-MO was designed against the 5′ start sequence of the *smn* gene (Gene Tools LLC.); 5′-CGACATCTTCTGCACCATTGGC-3′ (33). Zebrafish embryos were injected between the 1- and 4-cell stage. For direct evaluation of motor axon phenotype, we used embryos obtained from crossing TL/EK WT and *Tg(mnx:GFP)ml2* transgenic animals (53). Embryos were injected with either 4 or 6 ng of uba1-MO or 4 ng of *smn*-MO in aqueous solution containing 0.05% phenol red and 0.05% rhodamine-dextran. Six hours after injection, embryos were sorted according to homogeneity of rhodamine fluorescence, reflecting equal distribution of the injected MO solution. Quercetin (Sigma-Aldrich) treatment was performed at 6 hpf. In brief, quercetin solution (in DMSO) or DMSO (Sigma-Aldrich) was added to buffered embryo medium (final volume: 2 μl$_{DMSO}$/ml$_{medium}$) to obtain a final concentration of 50 μM. For immunostaining, fish (34 hpf) were dechorionated and fixed in 4% PFA overnight, dehydrated in methanol, rehydrated, and washed in PBS. After collagenase treatment (1 μg/ml; C-9891, Sigma-Aldrich) for 10 minutes at room temperature, embryos were blocked in PBST plus 1% DMSO plus 10% FCS, followed by overnight incubation in 500 μl blocking solution containing monoclonal mouse anti-zebrafish Synaptotagmin (znp-1) antibody (1:300; Developmental Studies Hybridoma Bank). After washing, fish were incubated in donkey anti-mouse secondary antibody labeled with

Alexa Fluor 488 (1:200; Invitrogen). Microscopical analysis was performed in 80% glycerol on micro slides using an Axioskop 2 fluorescence microscope (Zeiss). The length of each of the first 10 motor axons behind the yolk was analyzed and evaluated, as was the extent of abnormal branching (Supplemental Figure 4).

Zebrafish UBEI-41 experiments. UBEI-41 (BioGenova), on its own or with quercetin (Sigma-Aldrich), was dissolved in DMSO and added at 6 hpf to *Tg(mnx:GFP)ml2* embryos. The final amount of DMSO in the test groups was always 2 µl/ml in buffered embryo medium. Western blots were performed using the following antibodies: anti–β-actin (zebrafish) (rabbit polyclonal, 1:1,000; Anaspec); anti-Uba1 (mouse monoclonal, 1:1,000; Santa Cruz Biotechnology Inc.); anti–rabbit-HRP (1:10,000; GE Healthcare); anti–mouse-HRP (1:10,000; Sigma-Aldrich); anti–β-catenin (polyclonal rabbit, 1:1,000, C2206; Sigma-Aldrich). At 27 hpf, embryos were dechorionated, fixed in 4% PFA for 2 hours, and mounted in 70% glycerol. Motor nerves were assessed for abnormal trajectories using a Zeiss Axioscope A1 fluorescence microscope, and image stacks were taken using a Zeiss LSM710. For each embryo, 24 axons in 12 segments were analyzed. The observer was always blinded to the treatment.

SMA mouse quercetin experiments. Taiwanese mice and littermate controls were dosed daily with either 10 mg/kg quercetin (Sigma-Aldrich) or DMSO alone for a vehicle-only control via intraperitoneal injection. Mice were randomly assigned to treatment groups. Righting reflex tests were performed in order to assess neuromuscular function, as previously described (54). Muscle fibre diameter measurements were taken from phase-contrast micrographs of teased muscle fiber preparations using ImageJ software, as previously described (4). Motor neuron cell body counts were performed as previously described (32). NMJ pathology was assessed on whole-mount preparations of *levator auris longus* muscles, as described previously (5). Kaplan-Meier survival analyses were performed on DMSO and quercetin-treated mice as previously described (55). Organs were dissected and either fixed in 4% paraformaldehyde overnight for subsequent imaging, or were prepared for quantitative Western blotting.

Study approval. All required ethical approvals to acquire and distribute human patient tissue samples were obtained by the host biobanks. Tissue was provided in an anonymous fashion, with no identifying details apart from the age, sex, and genetic status of the patient. All animal studies were approved by the internal ethics committee at the University of Edinburgh and were performed under the authority of relevant project and personal licenses from the United Kingdom home office.

Statistics. All graphs are shown as mean ± SEM. All statistical analyses were completed using GraphPad Prism software. $P < 0.05$ was considered statistically significant for all analyses.

Address correspondence to: Thomas H. Gillingwater, Euan MacDonald Centre for Motor Neurone Disease Research and Centre for Integrative Physiology, University of Edinburgh, Edinburgh, EH8 9XD, United Kingdom. Phone: 44.0.131.6503724; E-mail: T.Gillingwater@ed.ac.uk.

1. Lefebvre S, et al. Identification and characterization of a spinal muscular atrophy-determining gene. *Cell.* 1995;80(1):155–165.
2. Wirth B. An update of the mutation spectrum of the survival motor neuron gene (SMN1) in autosomal recessive spinal muscular atrophy (SMA). *Hum Mutat.* 2000;15(3):228–237.
3. Burghes AH, Beattie CE. Spinal muscular atrophy: why do low levels of survival motor neuron protein make motor neurons sick? *Nat Rev Neurosci.* 2009;10(8):597–609.
4. Mutsaers CA, et al. Reversible molecular pathology of skeletal muscle in spinal muscular atrophy. *Hum Mol Genet.* 2011;20(22):4334–4344.
5. Murray LM, Comley LH, Thomson D, Parkinson N, Talbot K, Gillingwater TH. Selective vulnerability of motor neurons and dissociation of pre- and post-synaptic pathology at the neuromuscular junction in mouse models of spinal muscular atrophy. *Hum Mol Genet.* 2008;17(7):949–962.
6. Kariya S, et al. Reduced SMN protein impairs maturation of the neuromuscular junctions in mouse models of spinal muscular atrophy. *Hum Mol Genet.* 2008; 17(16):2552–2569.
7. Ling KK, Lin MY, Zingg B, Feng Z, Ko CP. Synaptic defects in the spinal and neuromuscular circuitry in a mouse model of spinal muscular atrophy. *PLoS One.* 2010;5(11):e15457.
8. Mentis GZ, et al. Early functional impairment of sensory-motor connectivity in a mouse model of spinal muscular atrophy. *Neuron.* 2011;69(3):453–467.
9. Imlach WL, Beck ES, Choi BJ, Lotti F, Pellizzoni L, McCabe BD. SMN is required for sensory-motor circuit function in Drosophila. *Cell.* 2012;151(2):427–439.
10. Hamilton G, Gillingwater TH. Spinal muscular atrophy: going beyond the motor neuron. *Trends Mol Med.* 2013;19(1):40–50.
11. Wishart TM, et al. SMN deficiency disrupts brain development in a mouse model of severe spinal muscular atrophy. *Hum Mol Genet.* 2010;19(21):4216–4228.
12. Shababi M, Habibi J, Yang HT, Vale SM, Sewell WA, Lorson CL. Cardiac defects contribute to the pathology of spinal muscular atrophy models. *Hum Mol Genet.* 2010;19(20):4059–4071.
13. Somers E, Stencel Z, Wishart TM, Gillingwater TH, Parson SH. Density, calibre and ramification of muscle capillaries are altered in a mouse model of severe spinal muscular atrophy. *Neuromuscul Disord.* 2012;22(5):435–442.
14. Hua Y, et al. Peripheral SMN restoration is essential for long-term rescue of a severe spinal muscular atrophy mouse model. *Nature.* 2011;478(7367):123–126.
15. Bowerman M, et al. Glucose metabolism and pancreatic defects in spinal muscular atrophy. *Ann Neurol.* 2012;72(2):256–268.
16. Schreml J, et al. Severe SMA mice show organ impairment that cannot be rescued by therapy with the HDACi JNJ-26481585. *Eur J Hum Genet.* 2013;21(6):643–652.
17. Zhang Z, et al. SMN deficiency causes tissue-specific perturbations in the repertoire of snRNAs and widespread defects in splicing. *Cell.* 2008;133(4):585–600.
18. Bäumer D, et al. Alternative splicing events are a late feature of pathology in a mouse model of spinal muscular atrophy. *PLoS Genet.* 2009;5(12):e1000773.
19. Lotti F, et al. An SMN-dependent U12 splicing event essential for motor circuit function. *Cell.* 2012; 151(2):440–454.
20. Praveen K, Wen Y, Matera AG. A Drosophila model of spinal muscular atrophy uncouples snRNP biogenesis functions of survival motor neuron from locomotion and viability defects. *Cell Rep.* 2012; 1(6):624–631.
21. Neveling K, et al. Mutations in BICD2, which encodes a golgin and important motor adaptor, cause congenital autosomal-dominant spinal muscular atrophy. *Am J Hum Genet.* 2013;92(6):946–954.
22. Ramser J, et al. Rare missense and synonymous variants in UBE1 are associated with X-linked infantile spinal muscular atrophy. *Am J Hum Genet.* 2008; 82(1):188–193.
23. Oprea GE, et al. Plastin 3 is a protective modifier of autosomal recessive spinal muscular atrophy. *Science.* 2008;320(5875):524–527.
24. Ackermann B, et al. Plastin 3 ameliorates spinal muscular atrophy via delayed axon pruning and improves neuromuscular junction functionality.

research article

Hum Mol Genet. 2013;22(7):1328–1347.

25. Ning K, et al. PTEN depletion rescues axonal growth defect and improves survival in SMN-deficient motor neurons. Hum Mol Genet. 2010;19(16):3159–3168.

26. Sanchez G, et al. A novel function for the survival motoneuron protein as a translational regulator. Hum Mol Genet. 2013;22(4):668–684.

27. Korhonen L, Lindholm D. The ubiquitin proteasome system in synaptic axonal degeneration: a new twist to an old cycle. J Cell Biol. 2004;165(1):27–30.

28. Chang HC, Hung WC, Chuang YJ, Jong YJ. Degradation of survival motor neuron protein is mediated via the ubiquitin/proteasome pathway. Neurochem Int. 2004;45(7):1107–1112.

29. Burnett BG, Muñoz E, Tandon A, Kwon DY, Sumner CJ, Fischbeck KH. Regulation of SMN protein stability. Mol Cell Biol. 2009;29(5):1107–1115.

30. Hsu SH, et al. Ubiquitin carboxyl-terminal hydrolase L1 (UCHL1) regulates the level of SMN expression through ubiquitination in primary spinal muscular atrophy fibroblasts. Clin Chim Acta. 2010; 411(23–24):1920–1928.

31. Chan YB, et al. Neuromuscular defects in a Drosophila survival motor neuron gene mutant. Hum Mol Genet. 2003;12(12):1367–1376.

32. Riessland M, et al. SAHA ameliorates the SMA phenotype in two mouse models for spinal muscular atrophy. Hum Mol Genet. 2010;19(8):1492–1506.

33. McWhorter ML, Monani UR, Burghes AH, Beattie CE. Knockdown of the survival motor neuron (Smn) protein in zebrafish causes defects in motor axon outgrowth and pathfinding. J Cell Biol. 2003; 162(5):919–931.

34. Balut CM, Loch CM, Devor DC. Role of ubiquitylation and USP8-dependent deubiquitylation in the endocytosis and lysosomal targeting of plasma membrane KCa3.1. FASEB J. 2011;25(11):3938–3948.

35. Cadigan KM. TCFs and Wnt/β-catenin signaling: more than one way to throw the switch. Curr Top Dev Biol. 2012;98:1–34.

36. Cashman NR, et al. Neuroblastoma x spinal cord (NSC) hybrid cell lines resemble developing motor neurons. Dev Dyn. 1992;194(3):209–221.

37. Zhang X, Peterson KA, Liu XS, McMahon AP, Ohba S. Gene regulatory networks mediating canonical Wnt signal directed control of pluripotency and differentiation in embryo stem cells [published online ahead of print March 15, 2013]. Stem Cells. doi:10.1002/stem.1371.

38. Aberle H, Bauer A, Stappert J, Kispert A, Kemler R. Beta-catenin is a target for the ubiquitin-proteasome pathway. EMBO J. 1997;16(13):3797–3804.

39. Park CH, Chang JY, Hahm ER, Park S, Kim HK, Yang CH. Quercetin, a potent inhibitor against β-catenin/Tcf signaling in SW480 colon cancer cells. Biochem Biophys Res Commun. 2005;328(1):227–234.

40. Gelebart P, et al. Constitutive activation of the Wnt canonical pathway in mantle cell lymphoma. Blood. 2008;112(13):5171–5179.

41. Asuthkar S, Gondi CS, Nalla AK, Velpula KK, Gorantla B, Rao JS. Urokinase-type plasminogen activator receptor (uPAR)-mediated regulation of WNT/β-catenin signaling is enhanced in irradiated medulloblastoma cells. J Biol Chem. 2012; 287(24):20576–20589.

42. Murase S, Mosser E, Schuman EM. Depolarization drives beta-catenin into neuronal spines promoting changes in synaptic structure and function. Neuron. 2002;35(1):91–105.

43. Li XM, et al. Retrograde regulation of motoneuron differentiation by muscle beta-catenin. Nat Neurosci. 2008;11(3):262–268.

44. Ojeda L, et al. Critical role of PI3K/Akt/GSK3β in motoneuron specification from human neural stem cells in response to FGF2 and EGF. PLoS One. 2011; 6(8):e23414.

45. Monani UR, et al. The human centromeric survival motor neuron gene (SMN2) rescues embryonic lethality in Smn−/− mice and results in a mouse with spinal muscular atrophy. Hum Mol Genet. 2000;

9(3):333–339.

46. Hsieh-Li HM, et al. A mouse model for spinal muscular atrophy. Nat Genet. 2000;24(1):66–70.

47. Mutsaers CA, Lamont DJ, Hunter G, Wishart TM, Gillingwater TH. Label-free proteomics identifies Calreticulin and GRP75/Mortalin as peripherally accessible protein biomarkers for spinal muscular atrophy. Genome Med. 2013;5(10):95.

48. Wishart TM, et al. Combining comparative proteomics and molecular genetics uncovers regulators of synaptic and axonal stability and degeneration in vivo. PLoS Genet. 2012;8(8):e1002936.

49. Young PJ, Le TT, Man NT, Burghes AHM, Morris GE. The relationship between SMN, the spinal muscular atrophy protein, and nuclear coiled bodies in differentiated tissues and cultured cells. Exp Cell Res. 2000;256(2):365–374.

50. Hanafusa H, et al. Leucine-rich repeat kinase LRRK1 regulates endosomal trafficking of the EGF receptor. Nat Commun. 2011;2:158.

51. Fuller HR, et al. The SMN interactome includes Myb-binding protein 1a. J Proteome Res. 2010; 9(1):556–563.

52. Bekkers JM, Stevens CF. NMDA and non-NMDA receptors are co-localized at individual excitatory synapses in cultured rat hippocampus. Nature. 1989;341(6239):230–233.

53. Flanagan-Steet H, Fox MA, Meyer D, Sanes JR. Neuromuscular synapses can form in vivo by incorporation of initially aneural postsynaptic specializations. Development. 2005;132(20):4471–4481.

54. Butchbach ME, Edwards JD, Burghes AH. Abnormal motor phenotype in the SMNDelta7 mouse model of spinal muscular atrophy. Neurobiol Dis. 2007; 27(2):207–219.

55. Lee AJ, Awano T, Park GH, Monani UR. Limited phenotypic effects of selectively augmenting the SMN protein in the neurons of a mouse model of severe spinal muscular atrophy. PLoS One. 2012; 7(9):e46353.